Available online at www.sciencedirect.com
SCIENCE DIRECT®
International Journal of Heat and Mass Transfer 49 (2006) 1631–1642
International Journal of HEAT and MASS TRANSFER
www.elsevier.com/locate/ijhmt

Estimation of heat transfer coefficients in oscillating flows: The thermoacoustic case

A. Piccolo [a,*], G. Pistone [b]

[a] Department of Physics, University of Messina, Contrada Papardo, Salita Sperone, 31-98166 S.Agata (Messina), Italy
[b] Department of Matter Physics and Advanced Physical Technologies, University of Messina, Contrada Papardo, Salita Sperone, 31-98166 S.Agata (Messina), Italy

Received 13 September 2004
Available online 9 January 2006

Abstract

The classical linear thermoacoustic theory is integrated through a numerical calculus with a simple energy conservation model to allow estimates of the optimal length of thermoacoustic heat exchangers and of the magnitude of the related heat transfer coefficients between gas and solid walls. This information results from the analysis of the temperature and heat flux density distributions inside a thermally isolated thermoacoustic stack. The effects of acoustic amplitude, plate spacing, plate thickness and Reynolds number on the heat transfer characteristics are examined. The results indicate that a net heat exchange between the acoustically oscillating gas and the solid boundary takes place only within a limited distance from the stack edges. This distance is found to be an increasing function of the plate spacing in the range ($0 \leqslant y_0/\delta_\kappa \leqslant 2$), becoming constant for $y_0/\delta_\kappa \geqslant 2$. The calculated dimensionless convective heat transfer coefficients, the Nusselt numbers, between gas and solid wall are comparable to those evaluated from classical correlations for steady laminar flow revised under the "Time-Average Steady-Flow Equivalent" (TASFE) and "root-mean-square Reynolds number" (RMSRe) models. Numerical results agree with measurements of the heat transfer coefficient found in literature to within 20%.

Keywords: Thermoacoustics; Heat; Sound; Heat exchangers; Convective coefficient

1. Introduction

The influence of sound or vibration on heat transfer has been the object of many research studies in the recent past [1] but until the eighties it remained just an academic problem. Over the last three decades, however, with the fast development of the thermoacoustic technology, this issue has become a problem of extraordinary engineering interest. In thermoacoustic engines (refrigerators and prime movers) intense sound waves (up to 180 dB) constrain fluid particles to undergo thermodynamic cycles which in traditional devices are performed by means of pistons, cranks, compressors, etc. with a great benefit in terms of simplicity, reliability and costs. Moreover, the employment of non-polluting working fluids makes thermoacoustic devices very attractive from an environmental point of view. A comprehensive review of the principles of thermoacoustic heat transport can be found in the tutorial article of Swift [2].

A thermoacoustic engine comprises four basic elements: a porous solid medium (stack); "hot" and "cold" heat exchangers facing both ends of the stack; an electroacoustic transducer (driver); a rigid and sealed plane wave resonator. As for all heat engines, the overall performance of a thermoacoustic device strongly depends upon the effectiveness of the heat exchangers. For small engines, where little heat transfer powers are required (<10 W), the heat exchangers usually relay only on thermal conduction. They can simply consist of thin parallel fins spanning the resonator at the stack ends and made of high thermal conductivity materials such as copper, silver or aluminium. For

* Corresponding author. Tel.: +39 090 3977311; fax: +39 090 3977480.
E-mail address: apiccolo@unime.it (A. Piccolo).

0017-9310/$ - see front matter © 2005 Elsevier Ltd. All rights reserved.
doi:10.1016/j.ijheatmasstransfer.2005.11.009

Nomenclature

a	speed of sound (m s^{-1})
A	cross sectional area of the stack open to the working fluid (m^2)
A_f	area of the fin cross section (m^2)
b	numerical factor
B_r	blockage ratio
c_P	isobaric specific heat of the gas (J kg^{-1} K^{-1})
c_S	specific heat of the plate material (J kg^{-1} K^{-1})
D	diameter of a circular duct (m)
D_h	hydraulic diameter (m)
$\dot{\mathbf{e}}$	time-averaged energy flux density (W m^{-2})
f_v	Rott's function
h	convective heat transfer coefficient (W m^{-2} K^{-1})
h_κ	complex thermal function
h_v	complex viscous function
$\dot{h}_x$	time-averaged enthalpy flux density along the x direction (W m^{-2})
i	imaginary unit
k	wave number (m^{-1})
K	thermal conductivity of the gas (W m^{-1} K^{-1})
K_f	thermal conductivity of the fin material (W m^{-1} K^{-1})
K_s	thermal conductivity of the plate material (W m^{-1} K^{-1})
l	half of the plate thickness (m)
L	length of a plate (m)
L_c	characteristic length (m)
L_f	fin length (m)
L_s	stack length (m)
L_T	thermal entry length (m)
m	fin constant (m^{-1})
M	Mach number
N_f	number of fins
Nu_D	Nusselt number involving D (or D_h) as characteristic distance
Nu_L	Nusselt number involving L (or L_c) as characteristic distance
P	perimeter of the cross section of a fin (m)
P_A	amplitude of the dynamic pressure at a pressure antinode (Pa)
P_m	mean pressure (Pa)
Pr	Prandtl number
P_0	amplitude of the dynamic pressure at the entrance of the stack (Pa)
P_1	amplitude of the dynamic pressure inside the stack (Pa)
$\dot{Q}$	rate of heat transfer (W)
$\dot{Q}_{\mathrm{exp}}$	measured values of $\dot{Q}$ (W)
$\dot{q}_x$	time-averaged heat flux density along the x direction (W m^{-2})
$\dot{q}_y$	time-averaged heat flux density along the y direction (W m^{-2})
Re_D	Reynolds number involving D as characteristic distance
Re_L	acoustic Reynolds number involving L as characteristic distance
Re_1	acoustic Reynolds number involving δ_v as characteristic distance
$Re_{1,D}$	acoustic Reynolds number involving D_h as characteristic distance
$Re_{1,L}$	acoustic Reynolds number involving L_c as characteristic distance
S	total gas solid heat exchange area in the heat exchanger (m^2)
S_b	area of the unfinned base surface (m^2)
t	time (s)
T_b	temperature of the base surface (K)
T_f	fin temperature (K)
T_m	time-averaged gas temperature (K)
T_{sh}	temperature of the hot end of the stack (K)
T_{sm}	time-averaged temperature of the stack plate (K)
T_1	amplitude of the acoustic temperature oscillations inside the stack (K)
u_0	amplitude of the acoustic particle velocity at the entrance of the stack (m s^{-1})
u_1	amplitude of the acoustic particle velocity inside the stack (m s^{-1})
$(\mathrm{UA})^{\mathrm{bf}}$	base-to-fin heat transfer coefficient (W K^{-1})
$(\mathrm{UA})^{\mathrm{exp}}$	heat exchanger-stack interelement heat transfer coefficient (W K^{-1})
x	axial coordinate (m)
x_1	particle displacement amplitude (m)
y	transverse coordinate perpendicular to the plate surface (m)
y_0	half distance between two plates (m)
z	transverse coordinate perpendicular to the x–y plane (m)

Greek symbols

δ_κ	thermal penetration depth of the gas (m)
δ_v	viscous penetration depth of the gas (m)
ΔL_{exc}	heat exchanger length along the x direction (m)
ΔL_s	stack length of the experimental apparatus in [9] (m)
ΔT_{exp}	measured values of the temperature difference $(T_b - T_{\mathrm{sh}})$ (K)
Δx	computation mesh size along the x direction (m)
Δy	computation mesh size along the y direction (m)
η_f	fin efficiency
κ	thermal diffusivity of the gas (m^2 s^{-1})
λ	wavelength of the sound wave (m)
v	kinematic viscosity (m^2 s^{-1})
ξ_s	mean distance of the stack from the centre of the resonator (m)

ρ_m	mean density of the gas (kg m^{-3})
ω	angular frequency of the sound wave (rad s^{-1})
Subscripts	
1	first order acoustic variable
A	acoustic amplitude at a pressure antinode
b	base
C	characteristic
D	diameter
exc	exchanger
exp	experimental
f	fin
h	hydraulic
L	length
m	mean, time averaged
max	maximum
P	isobaric
r	ratio
s	solid, stack
sh	"hot" side of the stack
sm	stack-mean
x	longitudinal
y	transversal
κ	thermal
v	viscous
Superscripts	
bf	base-to-fin
exp	experimental

greater thermal loads the finned-tube heat exchangers consisting of round tubes embedded in a matrix of parallel fins are used [3]. Optimal design depends on the understanding of the thermo-fluid dynamic processes controlling the heat transfer between the sound wave and the heat exchangers at the heat exchanger–stack junctions. Still today this issue is considered an unsolved problem and a major challenge in the design of heat exchangers for which established engineering methodologies are still lacking.

Standard design procedures for compact heat exchangers, in fact, generally refer to a steady and unidirectional flow of fluid while thermoacoustic heat exchangers are interested by an oscillatory flow with zero mean velocity. This circumstance has two important implications:

- An excessively long fin (along the longitudinal direction x of the particle acoustic oscillation) could only lead to additional thermoviscous losses without incrementing the surface area available for heat transfer. Conversely, a much too short fin could be ineffective in transferring the required thermal load. The optimal length of the heat exchanger fins should be of the order of the peak-to-peak acoustic displacement amplitude [2].
- Conventional steady flow heat transfer correlations cannot be directly applied for the estimation of the convective heat transfer coefficient (h) between gas and solid wall of thermoacoustic heat exchangers. Different approaches are currently proposed to overcome this limitation.

Swift [4] and Garrett [3] suggest that an approximate estimation of h can be achieved on the basis of a simple "boundary layer conduction heat transfer" model. The convective coefficient h should be roughly equal to the ratio K/δ_κ or, more exactly, to "some" root-mean-square (rms) value, the rate of heat transfer being expected to be sinusoidal in time:

$$h \approx \frac{1}{\sqrt{2}} \frac{K}{\delta_\kappa} \tag{1}$$

where K is the thermal conductivity of the gas and δ_κ $(= \sqrt{2\kappa/\omega})$ is the thermal penetration depth, the distance through which heat can diffuse in an acoustic cycle (κ and ω being respectively the thermal diffusivity and the angular frequency of the sound wave).

A similar result has been obtained analytically by Mozurkewich [5] for the case of planar pores on the basis of a one-dimensional model:

$$h \approx b \frac{K}{\delta_\kappa} \tag{2}$$

the numerical factor b resulting a mildly decreasing function of Prandtl number Pr with $b = 0.61$ for $Pr = 0.68$.

Another widely employed approach is the one in which the results of the standard steady-flow design methodology for compact heat exchangers are extended to the thermoacoustic case after suitable modifications. The main method based on this approach is the so called "Time-Average Steady-Flow Equivalent" (TASFE) approximation [6]. In this model the relevant steady flow heat transfer correlations are "recalibrated" for the oscillatory flow by taking their time average over an acoustic cycle. In the framework of this model some researchers [7] suggest to take the time-averaging over half an acoustic period justifying this on the assumption that the heat transfer rate is independent of the sign of the velocity. Other investigators [8], on the contrary, hypothesize that, due to the temperature discontinuities existing between the stack and the heat exchangers [9], the heat transfer rates during the positive and negative flow component of the cycle are not equivalent and suggest to introduce a correction factor for the Reynolds number in the time averaging computation. Relevant applications of the TASFE model to thermoacoustics have been carried out by Mozurkewich [10] who tested the model predictions based on Zukauska's single-tube steady cross flow correlation against experimental data involving heat transfer from geometrically simple heat exchangers placed immediately near the hot end of a thermoacoustic stack.

A similar method is the one proposed by Swift [11]—the "Root Mean Square Reynolds Number" (RMSRe) model—consisting in the direct substitution of the Reynolds numbers figuring in known steady flow correlations with their rms values.

The aim of the present work is to obtain through a numerical investigation information on the optimal length of thermoacoustic heat exchangers and on the magnitude of the related convective heat transfer coefficient between working gas and solid wall. The applied procedure, inspired to the approach proposed in [5,12] where the transverse heat transfer in thermoacoustics was analytically investigated, implements the classical linear thermoacoustic theory into an energy conservation scheme through a finite difference technique. The model allows in a very simple way to take into account the plate edge thermal effects (not described by the standard linear thermoacoustic theory) of a thermally isolated parallel-plate stack satisfying the "short-stack" approximation (see next section). As shown in [13,14], for a thermally isolated stack these edge effects consist of transverse (normal to the plate surface) time-averaged temperature gradients and heat fluxes. In steady state, in fact, energy balance forces the acoustically stimulated hydrodynamic energy flow in the gas to be returned back by thermal conduction in the solid plates; in the closed thermal loop that develops the plate edges act as real heat exchangers. The deriving results, therefore, can be directly applied to real configurations where two heat exchangers are generally placed in close proximity of both ends of the stack. The numerically computed heat transfer coefficients are compared with the results of classical steady flow correlations revised under the TASFE and RMSRe models and with experimental data available in literature.

2. Theory

The standard theory of thermoacoustics [2] is based on the simplifying assumption that at whatever cross section of a stack channel the time-averaged temperature of the gas, T_m, is spatially uniform (not dependent upon the transverse direction y) and equal to the time-averaged temperature of the adjacent solid surface, T_{sm}. The only dependence allowed for both gas and plates time-averaged temperatures is the one along the axial direction x, so precluding any net heat exchange between them. This hypothesis evidently fails near the stack terminations (or in the heat exchangers) where a time-averaged transverse heat diffusion can occur only as an effect of a non-zero time-averaged transverse temperature gradient.

In order to take into account for time-averaged transverse heat fluxes, in this work the linear thermoacoustic theory is integrated with a simple energy conservation model through a numerical calculus. The formulation takes advantage of the fact that for problems characterized by a periodic time dependence (like thermoacoustics) the time-averaged law of conservation of energy for a compressible viscous fluid is [15]

$$\nabla \cdot \dot{\mathbf{e}} = 0 \tag{3}$$

which implies that the time-averaged energy flux density, $\dot{\mathbf{e}}$, is the proper physical quantity to be considered for applying conservation of energy locally in the gas channel. For absolving to this task a finite difference technique is well suited where the quantitative results of standard linear theory for the components of the time-averaged energy flux density along the directions of interest may be used. It must be emphasized that for long enough plates (greater than the particle displacement length), these expressions are expected to hold accurately in the central regions of the stack where end-effects are negligible. Analogously, energy conservation can be imposed locally in the solid plates assuming thermal conduction as relevant mechanism of energy transport.

In order to formulate the basic equations to be used in the numerical simulation the governing equations of the linear thermoacoustic theory are briefly summarized for the simplified case of a parallel-plate stack. These equations are generally derived under the "short stack" approximation which can be synthesized as follows:

- the acoustic wavelength, λ, is much greater than the stack length, L_s, ($\lambda/2\pi \gg L_s$) so that pressure and velocity can be retained as constant over the stack;
- the acoustic field is non-significantly perturbed by the presence of the stack;
- the temperature difference across the stack is much smaller than the mean temperature so that the dependence of the thermophysical parameters of the gas on the temperature can be neglected.

The time-averaged hydrodynamic energy flow in the gas along the longitudinal direction x is the same as the time-averaged hydrodynamic enthalpy flow. If the equation of state of the gas is taken to be the ideal gas equation it results:

$$\dot{h}_x = \rho_m c_P \frac{\omega}{2\pi} \int_0^{2\pi/\omega} T_1 u_1 \, \mathrm{d}t = \frac{1}{2} \rho_m c_P Re\{T_1 \tilde{u}_1\} \tag{4}$$

where ρ_m is the mean density of the gas, c_P is the isobaric specific heat of the gas, T_1 is the first order amplitude of the temperature oscillation, u_1 is the first order amplitude of the acoustic particle velocity, t is the time, $Re\{\ \}$ signifies the real part and tilde indicates complex conjugation. To evaluate this quantity explicit expressions for the periodically time-varying quantities T_1 and u_1 inside the stack are required. If the stack material specific heat, c_S, is notably greater than c_P, the following expressions hold for T_1 and u_1 [11]:

$$T_1 = \frac{1}{\rho_m c_P}(1 - h_\kappa) P_1 - \frac{1}{\rho_m \omega^2} \frac{\mathrm{d}P_1}{\mathrm{d}x} \frac{\partial T_m}{\partial x} \left[\frac{(1 - h_\kappa) - Pr(1 - h_v)}{(1 - Pr)(1 - h_v)} \right] \tag{5}$$

$$u_1 = \frac{i}{\omega \rho_m} \frac{\mathrm{d}P_1}{\mathrm{d}x} (1 - h_v) \tag{6}$$

where

$$h_\kappa = \frac{\cosh[(1+\mathrm{i})y/\delta_\kappa]}{\cosh[(1+\mathrm{i})y_0/\delta_\kappa]}, \quad h_v = \frac{\cosh[(1+\mathrm{i})y/\delta_v]}{\cosh[(1+\mathrm{i})y_0/\delta_v]} \tag{7}$$

i being the imaginary unit, P_1 the local amplitude of the dynamic pressure, y_0 half distance between two plates and δ_v ($=\sqrt{2v/\omega}$) the viscous penetration depth (where v is the kinematical viscosity of the gas).

An approximate expression for the pressure derivative $\mathrm{d}P_1/\mathrm{d}x$ can be found observing that outside the stack the dissipative viscous effects can be retained negligible so for a half-wavelength resonator the harmonic acoustic field at the entrance of the stack can be described by the following expressions:

$$P_0 = P_A \sin k\xi_s, \quad \mathrm{i}u_0 = \mathrm{i}\frac{P_A}{\rho_m a}\cos k\xi_s \tag{8}$$

P_A being the amplitude of the dynamic pressure at a pressure antinode, k the wave number ($k = 2\pi/\lambda$), a the sound velocity and ξ_s the mean stack location (distance of the stack from the centre of the resonator). So, imposing continuity of volumetric velocity at the entrance of the stack the following expression is found for the pressure derivative:

$$\frac{\mathrm{d}P_1}{\mathrm{d}x} = \frac{u_0}{B_r}\frac{\rho_m\omega}{(1-f_v)} \tag{9}$$

where

$$f_v = \frac{\tanh[(1+\mathrm{i})y_0/\delta_v]}{[(1+\mathrm{i})y_0/\delta_v]} \tag{10}$$

and where the blockage ratio $B_r = 1/(1 + l/y_0)$ describes the porosity of the stack.

Being, by hypothesis, the stack acoustically non-intrusive the first of Eqs. (8) can reasonably describe also the pressure field inside the stack ($P_1 \approx P_0$). Thus, substituting this equation and Eq. (9) into Eqs. (5) and (6) and these last in Eq. (4) the following expression is found for the time-averaged convective enthalpy flux density along the x direction:

$$\dot{h}_x = \frac{1}{2B_r}\mathrm{Im}\left[\frac{(1-\tilde{h}_v)(1-h_\kappa)}{(1-\tilde{f}_v)}\right]P_0u_0 - \frac{c_P\rho_m}{2\omega B_r^2(1-Pr)}\frac{\partial T_m}{\partial x}\mathrm{Im}\left[\frac{(1-h_\kappa)(1-\tilde{h}_v)}{|1-f_v|^2}\right]u_0^2 \tag{11}$$

In the short stack approximation all quantities in this equation may be assumed independent of the axial coordinate x except T_m and its derivative; quantities enclosed in square brackets, on the other hand, depend only on the y coordinate reflecting the transverse variations of the acoustic velocity u_1 and of the oscillatory temperature T_1.

The conduction heat transfer along the axial direction $-K\partial T_m/\partial x$ is considered to be negligible in comparison with the hydrodynamic-one [13].

On the opposite hand, the transverse component of the energy flux density contains only the diffusive term

$$\dot{q}_y = -K\frac{\partial T_m}{\partial y} \tag{12}$$

where $\dot{q}_y$ is the time-averaged heat flux density along the transverse direction. This assumption is certainly valid near the plate surface where the fluid is at rest. Within the linear theory, however, it may be retained physically plausible also in regions far from the plate surface. The linearized equation of continuity, in fact, implies that, being $\partial/\partial x \sim 1/\lambda$ and $\partial/\partial y \sim 1/\delta_\kappa$, the velocity in the y direction is of order δ_κ/λ smaller than u_1 [2]. This entails, as verified in [16], very small hydrodynamic heat fluxes along the y direction which can be neglected respect to the diffusive-ones.

Since thermal conduction is the unique mechanism of energy transport inside the stack plates the time-averaged heat flux densities along the relevant directions are simply

$$\dot{q}_x = -K_s\frac{\partial T_{\mathrm{sm}}}{\partial x}, \quad \dot{q}_y = -K_s\frac{\partial T_{\mathrm{sm}}}{\partial y} \tag{13}$$

where K_s is the thermal conductivity of the plates material and having taken into account that, being by hypothesis $c_S \gg c_P$, the solid temperature oscillations are vanishingly small.

If the ratio of the plate spacing (and of the plate thickness) to the width in the transverse direction is very low (as in real cases) the energy flow along the z direction (perpendicular to the x–y plane) is negligible and the problem can be regarded as two-dimensional.

3. Numerical model

The simulation model system is a thermally isolated stack of parallel plates of length L_s located at position ξ_s in a half-wavelength gas filled resonator and subjected to a standing wave as shown in Fig. 1. As a stack is usually constituted by a set of identical plates, calculation is performed in a single channel of the stack, between a single pair of parallel plates. This region, enclosed by the dashed line, is shown magnified in Fig. 1. The simulation domain is further reduced by symmetry from half a gas duct to half a plate and is indicated by the light grey area together with the coordinate system used. The axis parallel to the plates is the x axis; $x = 0$ is chosen to be the beginning of the stack on the left. The y axis is perpendicular to the stack-plates; $y = 0$ is chosen to be the midpoint between the two adjacent plates.

The calculation of the steady-state two-dimensional time-averaged temperature distribution is performed using a finite difference methodology. To this end, the computational domain is subdivided using a rectangular grid. In the x direction the computation mesh size, Δx, is typically $0.0041L_s$ while in the y direction the computation mesh size, Δy, is typically $0.02y_0$. The set of finite-difference equations for the unknown quantities $T_m(x, y)$ and

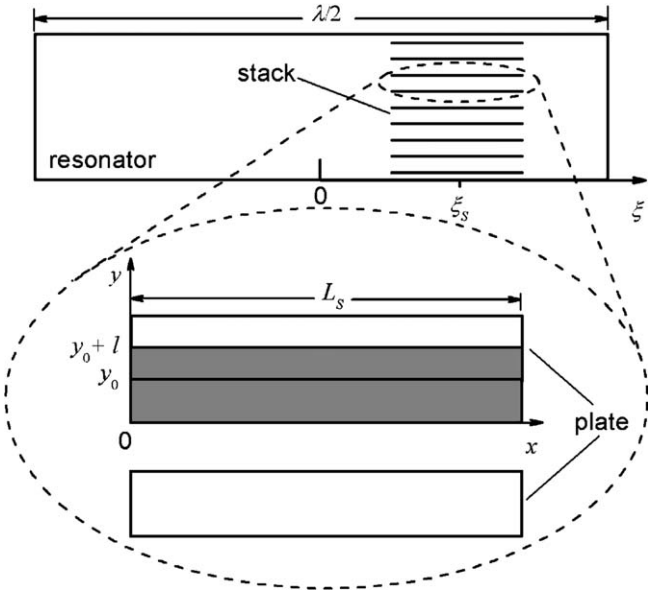

Fig. 1. Schematic illustration of a stack in a resonator and magnified region of two stack plates. The light grey area indicates the computation domain.

$T_{sm}(x, y)$ is then derived imposing conservation of energy at each nodal point of the computational grid making use of Eqs. (11) and (12) for the x and y components of the energy flux density in the gas and of Eqs. (13) for the analogues in the solid. Temperature spatial gradients are discretized in the standard way using first order nodal temperature differences.

The following boundary conditions are imposed:

- nodal lines at $y = 0$ and $y = y_0 + l$ are symmetry lines so

$$\left(\frac{\partial T_m}{\partial y}\right)_{y=0} = 0, \quad \left(\frac{\partial T_{sm}}{\partial y}\right)_{y=y_0+l} = 0 \tag{14}$$

- at the fluid–solid interface ($y = y_0$) the energy flux leaving (or entering) the gas must equal the energy flux entering (or leaving) the solid wall

$$K\left(\frac{\partial T_m}{\partial y}\right)_{y=y_0} = K_S\left(\frac{\partial T_{sm}}{\partial y}\right)_{y=y_0} \tag{15}$$

- for a thermally isolated stack no heat may leave or enter the stack diffusively across the plates terminations

$$\left(\frac{\partial T_{sm}}{\partial x}\right)_{x=0} = 0, \quad \left(\frac{\partial T_{sm}}{\partial x}\right)_{x=L_S} = 0 \tag{16}$$

- as far as the pore ends are concerned, suitable boundary conditions to apply at such sections for thermal isolation are available to the knowledge of the authors only in the work of Mozurkewich [5]. In his work the author suggests the requirement that the axial temperature gradient be uniform at the pore end and approaches the "critical gradient" [2] for which the integral of $\dot{h}_x$ over the section vanishes. This condition, however, does not preclude the existence of energy fluxes (both positive and negative) crossing the end section as only their sum must be zero. Furthermore, a non-zero uniform gradient cannot match a zero gradient which is found at the plate terminations according to (14). So, in this work the boundary condition that no energy may leave or enter the stack hydrodynamically across the pore ends is imposed simply setting

$$\dot{h}_x(x = 0) = 0, \quad \dot{h}_x(x = L_s) = 0 \tag{17}$$

even if this requirement is judged too strong by the author of [5].

The elements of the coefficient matrix associated to the resultant system of linear algebraic equations are calculated by a code developed by the authors (Digital Visual Fortran 6.0) and the system is solved using the relevant LAPACK library routines available online at [17]. Once the time-averaged temperature distribution is known, it can be substituted in Eqs. (11)–(13) to determine the energy flux distributions along the x and y directions both in the gas and in the plate.

The model, relying on the equations of the linear theory, does not take into account for nonlinear effects (presence of harmonics greater than the fundamental) or turbulent oscillatory flow, vortex generation, jetting (which can become relevant near the stack edges). These effects, on the other hand, could generate transverse heat transfer rates greater than the ones that would be obtained uniquely by thermal conduction, as they are calculated in the present work (Eq. (12)). Therefore, its applicability should be limited to acoustic Mach numbers ($M = P_A/\rho_m a^2$) and acoustic Reynolds numbers ($Re_1 = u_1\delta_v/\nu$) below respectively 0.1 and 550, the threshold values above which nonlinearity and turbulence become not negligible [18].

4. Results and analysis

Numerical simulations are carried out varying P_A, y_0 and l. The parameters of different runs are listed in Table 1.

In runs 1–18 helium at a mean temperature of 300 K and at a mean pressure of 10,000 Pa is assumed as working fluid. It is considered enclosed in a half-wavelength resonator 5.04 m length having a fundamental resonance frequency of 100 Hz. These operating conditions are chosen to facilitate the comparison with the test cases of Cao et al. [13] and Ishikawa et al. [14].

In run 19 test gas is air at a mean temperature of 333 K and at a mean pressure of 101,325 Pa. It is considered enclosed in a half-wavelength resonator 3.8 m length driven at a frequency of 44 Hz. These operating conditions are selected to reproduce the experimental conditions of Brewster et al. [9].

4.1. Comparison with other models

The test of the proposed model predictions against the results from previous numerical studies is illustrated in

Table 1
Parameters of selected simulations

Run	y_0/δ_κ	l/δ_κ	L_s/λ	ξ_s/λ	P_A/P_m
1	3.39	0.088	0.025	0.131	0.017
2	2	1.271	0.025	0.179	0.01–0.025
3	0.5–4	1.271	0.025	0.179	0.02
4	0.25–0.75	0.339	0.025	0.179	0.025
5	1–1.25	0.53	0.025	0.179	0.025
6	1.5–2	0.805	0.025	0.179	0.025
7	2.5–3	1.271	0.025	0.179	0.025
8	1	0.551	0.025	0.179	0.06
9	1.5	0.805	0.025	0.179	0.06
10	2	1.059	0.025	0.179	0.06
11	2.5	1.271	0.025	0.179	0.06
12	3	1.568	0.025	0.179	0.06
13	1	0.551	0.009	0.198	0.003–0.03
14	1	0.551	0.024	0.198	0.045–0.1
15	2	1.059	0.009	0.198	0.003–0.03
16	2	1.059	0.024	0.198	0.045–0.1
17	3	1.653	0.009	0.198	0.003–0.03
18	3	1.653	0.024	0.198	0.045–0.1
19	1.149	0.575	0.009	0.125	0.005–0.054

In runs 1–18 test gas = helium, mean temperature = 300 K, mean pressure = 10 kPa, resonator length = $\lambda/2$ = 5.04 m, resonance frequency = 100 Hz, plate material thermal conductivity = 10 W m^{-1} K^{-1}. In run 19 test gas = air, mean temperature = 333 K, mean pressure = 101.325 kPa, resonator length = $\lambda/2$ = 3.8 m, resonance frequency = 44 Hz, plate material thermal conductivity = 395 W m^{-1} K^{-1}.

Fig. 2 where the transverse component of the heat flux density at the gas–solid interface ($y = y_0$) for run 1 is compared with run 2 of Cao et al. [13] and run 7 of Ishikawa et al. [14]. It has to be noted that the parameters l and K_s have been set to arbitrarily values as in these works plate thickness and material have not been modeled. A quite perfect overlapping is found in spite of the fact that in these models different simulation domains and boundary conditions are specified. From this it could be argued that the motions of the fluid particles just outside a pore (modeled in [13,14] but not in this work) do not significantly affect the gas–solid heat transfer processes, at least at the pressure amplitudes involved. The simulation reproduces the result that the transverse heat flux is sharply peaked near the plate extremities being zero elsewhere. This is a clear evidence of the fact that a net heat exchange between fluid and solid takes place only at the plate edges. In particular, $|\dot{q}_y|$ exhibits a monotonic increase reaching a maximum when the end sections are approached: $\dot{q}_{y,\max} = |\dot{q}_y(x = 0, y = y_0)| = |\dot{q}_y(x = L_s, y = y_0)|$.

To get insight into the optimum length of the heat exchanger fins it is necessary to analyze the distance from the plate end over which a significant non-zero time-averaged heat transfer between solid and gas takes place. The results of this analysis are shown in Fig. 3 where the transverse component of the heat flux density at the solid boundary, normalized by $\dot{q}_{y,\max}$, is plotted as a function of the x coordinate normalized by the peak-to-peak particle displacement amplitude $2|\langle x_1\rangle| = 2|\langle u_1\rangle|/\omega$ (where brackets mean spatial average over the cross section) at selected P_A and y_0 values. For plate spacing larger than the thermal penetration depth ($y_0/\delta_\kappa > 1$) curves corresponding to different P_A are almost overlapping implying that the heat exchange length at the plate ends is linearly proportional to the particle displacement amplitude. The proportionality seems to be lost for very short plate spacing ($y_0/\delta_\kappa < 1$), the transverse heat flux profile being considerably more peaked. The dependence of the heat exchange length on the plate spacing is further analyzed in Fig. 4 where the distance from the plate edge over which the net heat transferred between gas and solid amounts to 90%, 95% and 98% of the total heat transferred is reported as

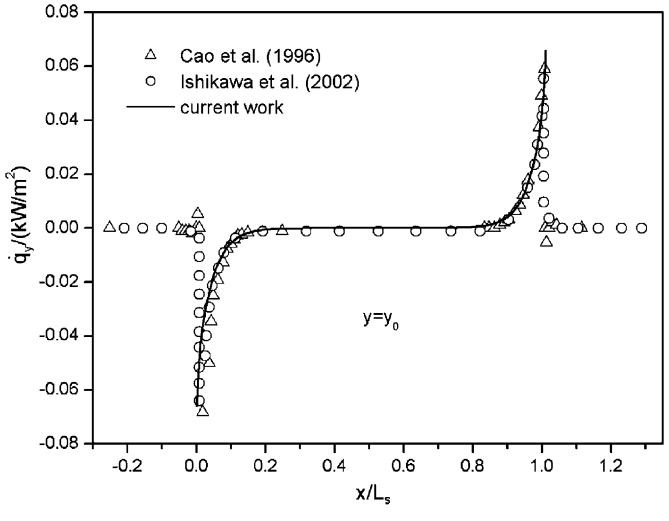

Fig. 2. Time-averaged heat flux density in the y direction at the plate surface ($y = y_0$) as a function of the position along the plate. Solid line is the heat flux density profile computed using the present model (run 1). Open triangles are numerical data from Ref. [13] (run 2). Open circles are numerical data from Ref. [14] (run 7). Positive values of $\dot{q}_y$ imply heat fluxes entering the plate while negative values of $\dot{q}_y$ imply heat fluxes leaving the plate.

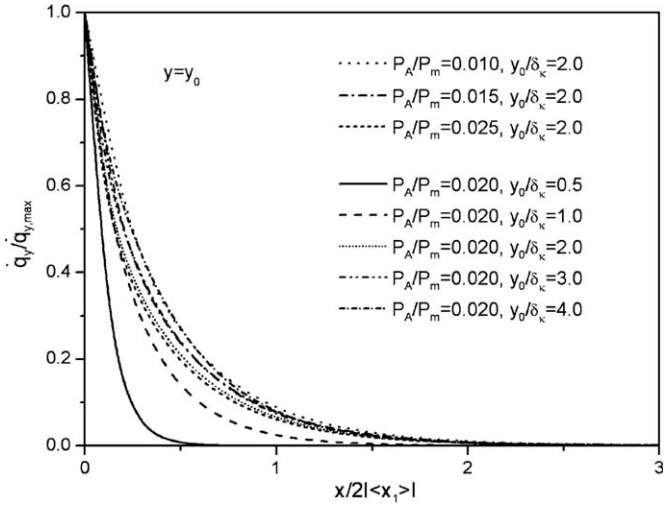

Fig. 3. Time-averaged heat flux density in the y direction at the plate surface ($y = y_0$) normalized by $\dot{q}_{y,\max}$ vs. $x/2I\langle x_1\rangle I$ at selected plate spacing and acoustic pressure amplitudes (runs 2–3).

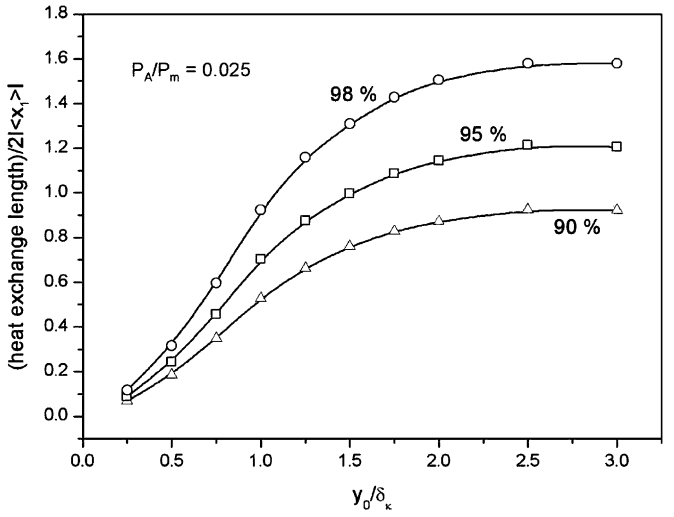

Fig. 4. Heat exchange length (distance from the plate edge over which the net heat transfer between gas and solid amount to 90%, 95% and 98% of the heat totally transferred) normalized by $2I\langle x_1\rangle I$ vs. plate spacing for $P_A/P_m = 0.025$ (runs 4–7).

a function of the plate spacing for $P_A/P_m = 0.025$ (P_m being the mean pressure of the gas). In the graph three regions are clearly distinguishable:

I for $y_0/\delta_\kappa < 1$ the length available for heat transfer increases very fast at increasing the plate spacing, still remaining lower than $2|\langle x_1\rangle|$;

II for $1 < y_0/\delta_\kappa < 2$ the curves exhibit a less marked growth. In this range for a heat exchange length equal to $2|\langle x_1\rangle|$ the net thermal power exchanged between gas and solid varies from 92% to 99% of the total power transferred;

III for $y_0/\delta_\kappa > 2$ the curves become flat denoting how the heat exchange length no more depends upon the plate spacing. In this range for a heat exchange length equal to $2|\langle x_1\rangle|$ the net thermal power exchanged between gas and solid amounts to 92% of the power totally transferred.

From the above considerations it follows that, as the plate spacing of real devices are generally found in range II, the peak-to-peak particle displacement amplitude can be conveniently assumed as useful length for the heat exchangers fins, as generally conjectured on heuristic grounds. The reduced heat exchange length found for very short plate spacing ($y_0/\delta_\kappa < 1$) is in agreement with the findings of Cao et al. [13] who ascribed this behavior to the improved thermal contact attending tightly spaced fins which reduces the phase lag between pressure and motion below the optimal value for which $\dot{h}_x$ peaks.

Numerical simulations performed at different plate thickness l (not shown) reveal that this parameter has little influence on the gas–solid heat exchange area: for a thermally isolated stack the plate simply serves as a duct which "closes" the energy flux path.

In order to compare the predictions of the standard correlations currently applied for estimation of the heat transfer coefficient between gas and solid walls of thermoacoustic heat exchangers reference is made to the well-known definition-law of h as reported in standard textbooks [19]:

$$h = \frac{K\left|\dfrac{\partial T_m}{\partial y}\right|_{y=y_0}}{|T_{\mathrm{sm}}(y_0) - T_m|} \tag{18}$$

which combines the Newton's law of cooling with the boundary condition that at the solid surface, being no fluid motion, energy transfer occurs only by conduction. This relation allows for estimation of the local convective heat transfer coefficient once the transverse temperature gradient is known, so it can be conveniently applied in the proposed numerical calculus. Since in relation (18) T_m represents the temperature of the bulk fluid in all performed simulations a plate spacing $y_0 \geqslant \delta_\kappa$ is chosen and T_m is evaluated at the centre of the pore: $T_m = T_m(y = 0)$.

In Fig. 5 the dependence of h on the normalized longitudinal coordinate $x/2|\langle x_1\rangle|$ at selected plate spacing is shown. The local convective coefficient varies with x attaining, at a distance greater than $2|\langle x_1\rangle|$, a constant value which depends, in turn, on the plate spacing; this dependence disappears for $y_0/\delta_\kappa > 2.5$, the curves almost overlapping each other.

Once the local h values are determined a spatially averaged convective heat transfer coefficient can be calculated as

$$\bar{h} = \frac{1}{L_c}\int_{L_c} h\,\mathrm{d}x \tag{19}$$

where overbar indicates spatial averaging and where, as suggested by the previous analysis, the characteristic length L_c is chosen equal to the peak-to-peak particle displacement amplitude: $L_c = 2|\langle u_1\rangle|/\omega$. Values thus obtained are

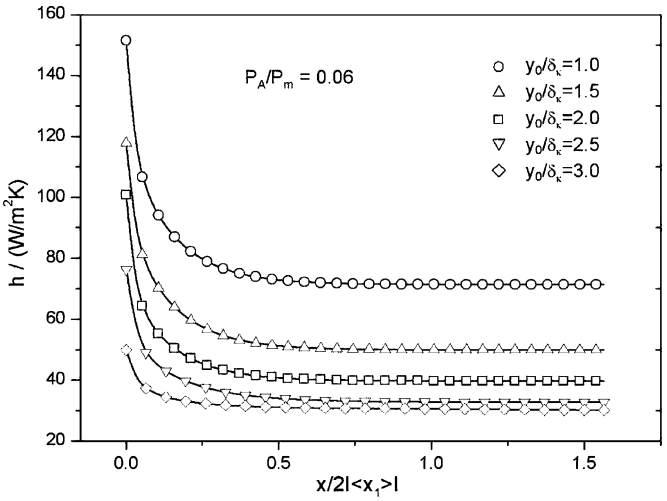

Fig. 5. Convective heat transfer coefficient between gas and solid vs. $x/2I\langle x_1\rangle I$ at selected plate spacing for $P_A/P_m = 0.06$ (runs 8–12).

converted to dimensionless average Nusselt numbers, $\overline{Nu}$, through the well-known relation

$$\overline{Nu}_L = \frac{\bar{h}L_c}{K} \tag{20}$$

Results are shown in Fig. 6 where the Nusselt number values deriving with this procedure (open circles, open triangles and open squares + continuous lines) are reported as a function of the acoustic Reynolds number at selected plate spacing. The acoustic Reynolds number is defined in terms of L_c and of the amplitude of the acoustic velocity in the bulk fluid outside the boundary layer:

$$Re_{1,L} = \frac{u_1 L_c}{\nu} \tag{21}$$

In the calculus procedure the acoustic amplitude at the centre of the pore, $u_1(y = 0)$, is substituted for u_1. Since in all simulations $y_0 \geqslant \delta_\nu$ this value should represent a good approximation of the velocity of the bulk fluid.

The comparison of the simulation data with the predictions of the TASFE and RMSRe models is carried out considering the standard correlation for steady laminar flow that allows calculation of the Nusselt number averaged over a plate of length L [19]:

$$\overline{Nu} = 0.664 Pr^{1/3} Re_L^{1/2} \tag{22}$$

Re_L being the Reynolds number involving L as characteristic distance.

To obtain the corresponding TASFE correlation a sinusoidally oscillating velocity, $u_1\sin(\omega t)$, is assumed and substituted in Eq. (22). The time average over one-half cycle of the resulting time-dependent Nusselt number is then numerically computed:

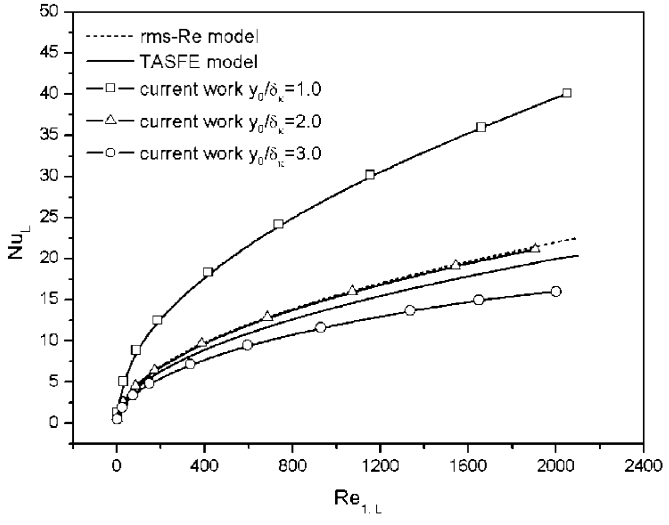

Fig. 6. Numerical results (open circles, open triangles and open squares + continuous lines) for the Nusselt number vs. acoustic Reynolds number (runs 13–18) compared with the predictions of the classical correlation for steady laminar flow over plates revised under the TASFE (continuous line) and RMSRe (dashed line) models.

$$\overline{Nu}_L = \frac{1}{\pi}\int_0^{\pi/\omega} (0.644 Pr^{1/3} Re_{1,L}^{1/2} \sin\omega t)\,\mathrm{d}t = 0.507 Pr^{1/3} Re_{1,L}^{1/2} \tag{23}$$

The plot of this law vs. the acoustic Reynolds number is shown in Fig. 6 (solid line).

As far as the RMSRe model is concerned the corresponding correlation is

$$\overline{Nu}_L = 0.664 Pr^{1/3}\left(\frac{Re_{1,L}}{\sqrt{2}}\right)^{1/2} = 0.558 Pr^{1/3} Re_{1,L}^{1/2} \tag{24}$$

The plot of this law vs. the acoustic Reynolds number is shown in Fig. 6 (dotted line).

The results indicate that at large plate spacing ($y_0/\delta_\kappa > 2$) the numerically computed values of the Nusselt number agree quite well with the predictions of the TASFE and RMSRe models, relatively to the correlation considered. A quite perfect matching is found between the RMSRe model and the proposed methodology for $y_0/\delta_\kappa = 2$; at the highest Reynolds number investigated the disagreement among the three models is less than 40%. The numerical calculus results deviate considerably from those of the other models for narrow plate spacing ($y_0/\delta_\kappa < 2$). This result is not surprising since Eq. (22) is defined for external flow conditions so its applicability to thermoacoustic heat exchangers should be limited to highly spaced fins ($y_0/\delta_\kappa > 2$).

In the next subsection, where a comparison with experimental data is proposed, the Hausen correlation [19] is considered as a first attempt to take into account both for fin spacing and fin length.

4.2. Comparison with experimental data

The validation of the model against experimental data has been carried out making reference to the work of Brewster et al. [9] where experimental measurements of the rate of heat transfer and of the temperature differences between adjoining "hot" stack-end and "hot" heat exchanger of a thermoacoustic refrigerator are reported. The heat exchanger is of the parallel-plate conductive type so these data can be conveniently converted in a form suited to make comparison. For the parallel-fin conductive heat exchanger elementary analysis reported in standard textbooks provide the following expression for the heat transfer rate between the fluid and the wall:

$$\dot{Q} = \left(\sum_{i=1}^{N_f} hPL_{fi}\eta_{fi} + hS_b\right)(T_b - T_m) \tag{25}$$

where N_f is the number of fins, P is the perimeter of the cross section of a fin, L_{fi} is the length of the ith fin along the z direction (see Fig. 7), S_b is the area of the unfinned base surface where fins are attached and T_b is the temperature of the base surface. The fin efficiency, η_{fi}, is defined as the ratio of the actual heat transfer to the "maximum" heat transfer rate that would occur when both fin and base

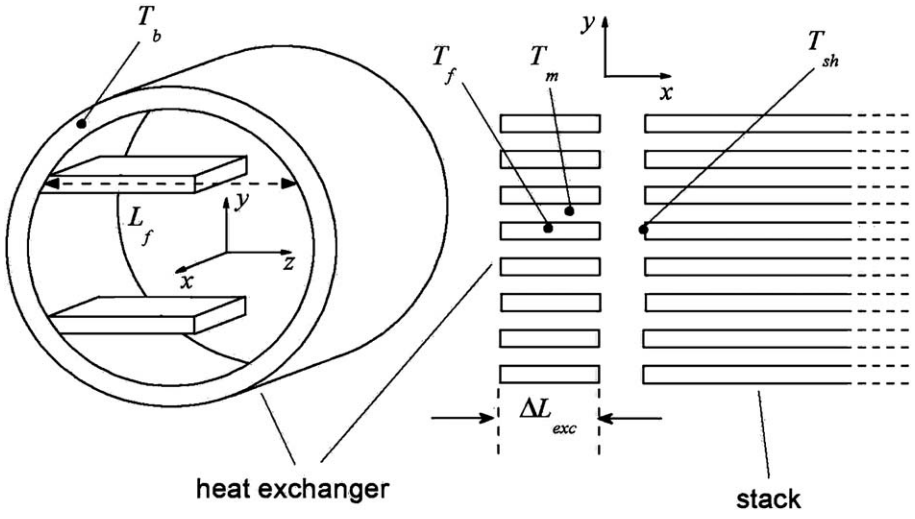

Fig. 7. Sketch of the conductive heat exchanger with indication of the temperatures.

surface are at the same base temperature. Analysis of straight fins with adiabatic centerline provide the following expression for η_{fi}:

$$\eta_{fi} = \frac{\tanh(mL_{fi}/2)}{mL_{fi}/2}, \quad m = \sqrt{\frac{hP}{A_f K_f}} \tag{26}$$

where A_f is the area of a fin cross section and K_f is the thermal conductivity of the fin material.

In Eq. (25) the temperature differences $(T_b - T_m)$ are involved while in [9] the experimentally measured values

$$\Delta T_{\exp} = (T_b - T_{\mathrm{sh}}) \tag{27}$$

are available, T_{sh} being the temperature of the hot end of the stack facing the hot heat exchanger (see Fig. 7). The simple calculation outlined in the Appendix, however, allows to convert the measured values (27) into the differences $(T_b - T_m)$ required for substitution in (25); the conversion formula is

$$(T_b - T_m) = \dot{Q}_{\exp}\left\{\left[\frac{\Delta T_{\exp}}{\dot{Q}_{\exp}} - \frac{1}{(\mathrm{UA})^{\mathrm{bf}}}\right]\left(\frac{4|u_1|y_0}{\pi\omega\Delta L_{\mathrm{exc}}\delta_\kappa}\right) + \frac{1}{(\mathrm{UA})^{\mathrm{bf}}}\right\} \tag{28}$$

where $\dot{Q}_{\exp}$ are the experimental values of the rate of heat transfer, ΔL_{exc} is the length of the heat exchanger fins along the longitudinal direction x and where $1/(\mathrm{UA})^{\mathrm{bf}}$, the thermal resistance of the base-to-fin path, has been estimated in [9] to be $\sim 1/12\ \mathrm{K\ W^{-1}}$.

In this way, the values of the convective heat transfer coefficient are those which solve Eq. (25) in correspondence of each couple of measured values $\dot{Q}_{\exp}$, $\Delta T_{\exp}$.

The h data thus obtained are converted to non-dimensional Nusselt number based on the hydraulic diameter of the pore D_h (=$4y_0$)

$$\overline{Nu}_D = \frac{\bar{h}D_h}{K} \tag{29}$$

Results are plotted in Fig. 8 (full circles), along with the predictions of the numerical model (open circles + continuous line), as a function of the acoustic Reynolds number

$$Re_{1,D} = \frac{u_1 D_h}{\nu} \tag{30}$$

In the simulations the stack and the heat exchangers of the experimental apparatus (of length respectively ΔL_s and ΔL_{exc}) are modeled by a thermally isolated stack of length $L_s = \Delta L_s + 2\Delta L_{\mathrm{exc}}$, as in the proposed model the role of the heat exchangers is played by the stack edges. The convective heat transfer coefficient, moreover, is calculated averaging the local h values over the fixed length ΔL_{exc}.

In order to test the predictions of the TASFE and RMSRe models the Hausen correlation [19] for laminar flow in the entry region of ducts is considered:

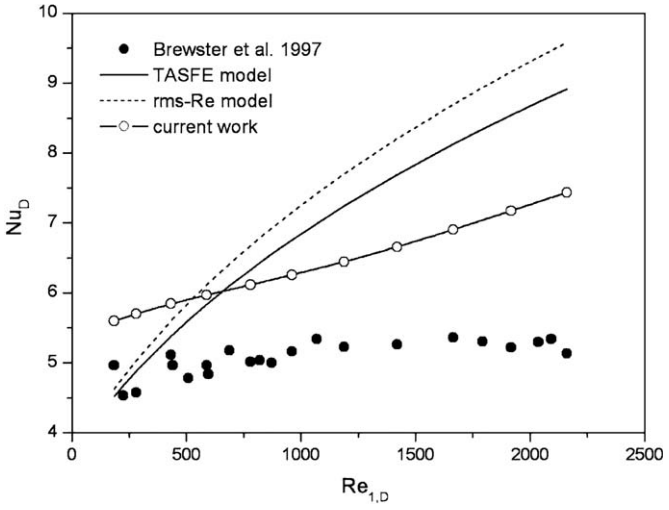

Fig. 8. Numerically computed Nusselt number (open circles + line) for run 19 compared with the experimental measurements of Brewster et al. [9] (full circles) and the predictions of the Hausen correlation revised under the TASFE (continuous line) and RMSRe (dashed line) models.

$$\overline{Nu}_D = 3.66 + \frac{0.0668(D/L_T)PrRe_D}{1 + 0.04[(D/L_T)PrRe_D]^{2/3}} \quad (31)$$

D being the diameter of the circular duct, L_T the thermal entry length and Re_D the Reynolds number involving D as characteristic distance. This correlation is preferred to Eq. (22) as for the involved geometry and experimental conditions it results $y_0/\delta_\kappa \approx 1$, so the fins cannot be considered as highly spaced.

To find the corresponding TASFE correlation the time-average of Eq. (31) over one-half the acoustic period is computed

$$\overline{Nu}_D = \frac{1}{\pi}\int_0^{\pi/\omega}\left\{3.66 + \frac{0.0668(D_h/\Delta L_{\text{exc}})PrRe_{1,D}\sin\omega t}{1 + 0.04[(D_h/\Delta L_{\text{exc}})PrRe_{1,D}\sin\omega t]^{2/3}}\right\}\mathrm{d}t \quad (32)$$

The results of the numerical integration can be parameterized in the investigated range ($200 \leqslant Re_{1,D} \leqslant 2200$) as

$$\overline{Nu}_D = 2.8731 + 0.11432(Re_{1,D})^{1/2} + 0.00035(Re_{1,D}) \quad (33)$$

and are represented in Fig. 8 by the continuous line.

In the same figure the predictions of Eq. (31) revised under the RMSRe model (dashed line)

$$\overline{Nu}_D = 3.66 + \frac{0.0668(D_h/\Delta L_{\text{exc}})Pr(Re_{1,D}/\sqrt{2})}{1 + 0.04[(D_h/\Delta L_{\text{exc}})Pr(Re_{1,D}/\sqrt{2})]^{2/3}} \quad (34)$$

are also shown. In plotting Eqs. (32) and (34) the thermal entry length, L_T, has been identified with the heat exchanger fin length ΔL_{exc}.

The results of the numerical model seem to agree better than the TASFE and RMSRe models predictions based on Eq. (31) with the experimental data of Brewster et al. The mean deviations from the measured Nu_D values are respectively 20% for the numerical model, 32% for the TASFE model and 39% for the RMSRe model, even if the last two models seem to work better at low acoustic Reynolds numbers ($Re_{1,D} < 700$) where the deviations from the experimental data reduce respectively to 6 and 7%. For higher Reynolds numbers the TASFE- and RMSRe-modified Hausen correlation overestimate both the measured and numerical data.

In evaluating these results some remarks have to be pointed out:

- the stack used in [9] is a ceramic lattice of parallel square ducts so its performance could be different from that of a parallel-plate stack (used in the numerical simulations) [20];
- at the involved acoustic Reynolds numbers the peak-to-peak particle displacement amplitude is always greater than the heat exchanger length so the procedure of averaging the local h values over the fixed length ΔL_{exc} could be not appropriate;
- the conversion formula (28) relies on the results of the "complete heat-exchange" theory [9] and of the "thermal boundary-layer" theory [4] so its correctness is subordinate to the validity of these theories;
- In Eqs. (32) and (34) the identification of the thermal entry length L_T with the heat exchanger length ΔL_{exc} is arbitrary.

5. Conclusions

In this paper a numerical calculus scheme has been developed by implementing the simplified linear thermoacoustic theory—the short stack approximation–into a simple energy conservation model through a finite difference methodology. The model allows to enquire on the optimal length of thermoacoustic heat exchangers and on the magnitude of the related heat transfer coefficients between gas and solid walls. Results show that for plate spacing falling in the range $1 < y_0/\delta_\kappa < 2$ the peak-to-peak particle displacement amplitude can be conveniently assumed as optimal length of heat exchangers fins; this length decreases significantly at short plate spacing ($y_0/\delta_\kappa < 1$), a circumstance that should be taken into account in the design procedures.

The calculated dimensionless convective heat transfer coefficients, the Nusselt numbers, between gas and solid wall are comparable to those evaluated from classical correlations for steady laminar flow revised under the TASFE and RMSRe models. Precisely, the comparative analysis of the results suggest that at large plate spacing ($y_0/\delta_\kappa > 2$) correlations for external flow conditions can be usefully applied while at short plate spacing ($y_0/\delta_\kappa < 2$) correlations which take into account the effect of plate spacing are more suited. The predictions of the numerical model are found to be within 20% the experimental data of Brewster et al. [9]; this deviation is lower than those arising from the TASFE- and RMSRe-modified Hausen correlations. Indeed, the identification of the thermal entry length with the heat exchanger fin length in Eqs. (32) and (34) may result quite arbitrary and needs more analysis. At this stage, however, it constitutes simply a first attempt to take into account both for fin spacing and fin length in the evaluation of the convective heat transfer coefficients between gas and solid wall of tightly spaced heat exchanger fins.

Acknowledgement

The authors gratefully thank Dr. Giovanni Finocchio for critical conversations.

Appendix

For application of Eq. (25) it was noted earlier (Section 4.2) that the experimentally measured temperature differences ($T_b - T_{\text{sh}}$) must be converted into the differences ($T_b - T_m$). A procedure for carrying this out, based on the analysis of the series of heat paths by which the heat is transferred from the base of the heat exchanger to the stack, is outlined in this appendix.

From the measured values of $\dot{Q}$ and $(T_b - T_{sh})$, the heat exchanger-stack interelement heat transfer coefficient can be calculated from

$$\dot{Q}_{exp} = (UA)^{exp} \Delta T_{exp} \tag{A1}$$

On the other hand, from a simplified analysis based on the heat conduction equation the authors of [9] have derived an expression for the thermal resistance of the base-to-fin path $1/(UA)^{bf}$; for the involved geometry it resulted $(UA)^{bf} = 12\ W\ K^{-1}$. In this way, the rate of heat transfer can be also expressed as

$$\dot{Q} = (UA)^{bf}(T_b - T_f) \tag{A2}$$

where T_f is the temperature of the fins at the centre of the resonator. Combining Eqs. (A1) and (A2) it follows

$$\dot{Q} = \left[\frac{1}{(UA)^{exp}} - \frac{1}{(UA)^{bf}}\right]^{-1} (T_f - T_{sh}) \tag{A3}$$

The same temperature difference appears in the expression of $\dot{Q}$ that the authors of [9] have derived on the basis of the "complete heat-exchanger" theory

$$\dot{Q} = \frac{2}{\pi} A c_P \rho_m |u_1| (T_f - T_{sh}) \tag{A4}$$

where A is the cross sectional area of the stack open to the working fluid. For the details of the derivation of this formula the reader is addressed to [9]. This expression can be compared to the one put forward by Swift on the basis of the "thermal boundary-layer" theory [4]

$$\dot{Q} = KS \left.\frac{\partial T_m}{\partial y}\right|_{y_0} \approx KS \frac{(T_f - T_m)}{\delta_\kappa} = \frac{KA\Delta L_{exc}}{y_0 \delta_\kappa} (T_f - T_m) \tag{A5}$$

where S is the total gas–solid surface area available for heat transfer in the heat exchanger and having taken into account that for rectangular geometries $S = \Delta L_{exc} A / y_0$. Equating this equation to Eq. (A4) and rearranging

$$(T_f - T_{sh}) = \frac{\pi \omega \Delta L_{exc} \delta_\kappa}{4|u_1| y_0} (T_f - T_m) \tag{A6}$$

that, substituted into Eq. (A3) yields

$$\dot{Q} = \left[\frac{1}{(UA)^{exp}} - \frac{1}{(UA)^{bf}}\right]^{-1} \left(\frac{\pi \omega \Delta L_{exc} \delta_\kappa}{4|u_1| y_0}\right) (T_f - T_m) \tag{A7}$$

Finally, combining this equation with Eq. (A2) and rearranging

$$(T_b - T_m) = \dot{Q} \left\{ \left[\frac{1}{(UA)^{exp}} - \frac{1}{(UA)^{bf}}\right] \left(\frac{4|u_1| y_0}{\pi \omega \Delta L_{exc} \delta_\kappa}\right) + \frac{1}{(UA)^{bf}} \right\} \tag{A8}$$

which is the same of Eq. (28) if $\dot{Q}_{exp}$ and $\dot{Q}_{exp}/\Delta T_{exp}$ are substituted respectively for $\dot{Q}$ and $(UA)^{exp}$.

References

[1] R.M. Fand, P. Cheng, The influence of sound on heat transfer from cylinder in cross-flow, Int. J. Heat Mass Transfer 6 (1963) 571–596, and references therein.

[2] G.W. Swift, Thermoacoustic engines, J. Acoust. Soc. Amer. 84 (8) (1988) 1145–1180.

[3] S.L. Garret, D.K. Perkins, A. Gopinath, Thermoacoustic refrigerator heat exchangers: design, analysis and fabrication, in: G.F. Hewitt (Ed.), Proceedings of the Tenth International Heat Transfer Conference, Brighton, UK, 1994, pp. 375–380.

[4] G.W. Swift, Analysis and performance of a large thermoacoustic engine, J. Acoust. Soc. Amer. 92 (3) (1992) 1551–1563.

[5] G. Mozurkewich, Time average temperature distribution in a thermoacoustic stack, J. Acoust. Soc. Amer. 103 (1) (1998) 380–388.

[6] P.D. Richardson, Effects of sound and vibration on heat transfer, Appl. Mech. Rev. 20 (1967) 201–217.

[7] E. Matthew, E. Pose, S.L. Garrett, Performance measurements on a thermoacoustic refrigerator driven at high amplitudes, J. Acoust. Soc. Amer. 107 (5) (2000) 2480–2486.

[8] I. Peak, J.E. Braun, L. Mongeau, Heat transfer coefficients of heat exchangers in the thermoacoustic coolers, in: Proceedings of the International Congress of Refrigeration, Washington, DC, 2003, pp. 1–8.

[9] J.R. Brewster, R. Raspet, H.E. Bass, Temperature discontinuities between elements of thermoacoustic devices, J. Acoust. Soc. Amer. 102 (6) (1997) 3355–3360.

[10] G. Mozurkewich, Heat transfer from transverse tubes adjacent to a thermoacoustic stack, J. Acoust. Soc. Amer. 110 (2) (2001) 841–847.

[11] G.W. Swift, Thermoacoustics: a unifying perspective for some engines and refrigerators, fourth draft, Los Alamos National Labs, New Mexico, 1999, pp. 175.

[12] G. Mozurkewich, A model for transverse heat transfer in thermoacoustic, J. Acoust. Soc. Amer. 103 (6) (1998) 3318–3326.

[13] N. Cao, J.R. Olson, G.W. Swift, S. Chen, Energy flux density in a thermoacoustic couple, J. Acoust. Soc. Amer. 99 (6) (1996) 3456–3464.

[14] H. Ishikawa, D.J. Mee, Numerical investigations of flow and energy fields near a thermoacoustic couple, J. Acoust. Soc. Amer. 111 (2) (2002) 831–839.

[15] L.D. Landau, E.M. Lifshitz, Fluid Mechanics, first ed., Pergamon, London, 1959, pp. 184.

[16] A.O. Santillan, R.R. Bullosa, Space dependence of acoustic power and heat flux in the thermoacoustic effect, Int. Commun. Heat Mass Transfer 22 (4) (1995) 539–548.

[17] http://www.netlib.org/lapack.

[18] P. Merkli, H. Thomann, Transition to turbulence in oscillating pipe, J. Fluid Mech. 68 (1975) 567–579.

[19] F. Incoprera, D. Dewitt, Fundamentals of Heat and Mass Transfer, third ed., Wiley and Sons, New York, 1996, pp. 130, 320, 395, 495.

[20] W.P. Arnott, H.E. Bass, R. Raspet, General formulation of thermoacoustics for stacks having arbitrarily shaped pore cross sections, J. Acoust. Soc. Amer. 90 (1991) 3228–3237.